Dyes and Pigments 207 (2022) 110635

Contents lists available at ScienceDirect

Dyes and Pigments

journal homepage: www.elsevier.com/locate/dyepig

Combined use of phosphonium-erythrosin B-based nanoGUMBOS, UV–Vis spectroscopy, and chemometrics for discrimination and quantification of proteins

Ana M.O. Azevedo [a], Clara Sousa [b,*], S. Sofia M. Rodrigues [a], Mi Chen [c], Caitlan E. Ayala [c], Rocío L. Pérez [c,d], João L.M. Santos [a], Isiah M. Warner [c], M. Lúcia M.F.S. Saraiva [a,**]

[a] LAQV, REQUIMTE, Departacnto de Ciências Químicas, Laboratório de Química Aplicada, Faculdade de Farmácia, Universidade do Porto, Rua Jorge Viterbo Ferreira 228, 4050-313, Porto, Portugal

[b] Universidade Católica Portuguesa, CBQF – Centro de Biotecnologia e Química Fina – Laboratório Associado, Escola Superior de Biotecnologia, Rua Diogo Botelho 1327, 4169-005, Porto, Portugal

[c] Department of Chemistry, Louisiana State University, Baton Rouge, LA, 70803, United States

[d] Department of Chemistry and Biochemistry, Georgia Southern University, Statesboro, GA, 30458, United States

ARTICLE INFO

Keywords:
Chemometrics
NanoGUMBOS
Proteins
Ultraviolet–visible spectroscopy

ABSTRACT

Nanoparticles derived from a group of uniform materials based on organic salts (nanoGUMBOS) are considered promising candidates for protein analysis due to their facile synthesis in aqueous media and high tunability. In this study, a phosphonium-erythrosin B-based nanoGUMBOS (i.e., $[P_{4444}]_2$[EB]) was prepared using an ultrasound-assisted reprecipitation method, and its ability to discriminate and quantify proteins was evaluated. Sonication time (30 s, 5 min, and 15 min) and cyclodextrin templating (α-, 2-HP-β-, and γ-CD) were investigated for their effects on discrimination performance of synthesized nanomaterial. Six proteins (albumin, hemoglobin, trypsin, catalase, lysozyme, and cytochrome *c*) with different abundance levels and physicochemical properties were selected as target analytes. Absorbance response patterns generated from interactions between $[P_{4444}]_2$[EB] nanoGUMBOS and proteins were analyzed using partial least squares discriminant analysis. Percentages of correct protein discrimination ranged from 94.6 to 99.6%, with the latter being the best result obtained using non-templated nanoGUMBOS formed after 5 min sonication. Under optimized conditions, it was possible to discriminate all protein samples with percentages of correct assignments greater than 90% for concentrations as low as 2.0 μg mL^{-1}. The discrimination capability of synthesized nanoGUMBOS was further evaluated using mixtures of different ratios of lysozyme, cytochrome *c*, and hemoglobin. Finally, partial least squares models were developed for protein quantification and the best performance was observed for albumin. Results support potential use of $[P_{4444}]_2$[EB] nanoGUMBOS in combination with ultraviolet–visible spectroscopy and chemometrics for qualitative and quantitative analyses of individual proteins and mixtures of proteins.

1. Introduction

Simultaneous analyses of multiple protein biomarkers has been recognized as a valuable tool for improving diagnostic accuracy, predicting long-term outcomes, and guiding treatment decisions [1,2]. Thus, considerable efforts have been made to develop rapid and sensitive methods for detection and quantification of proteins using a multiplexed approach. Mass spectrometry is one of the most widely used analytical tools due to the ability to measure hundreds of proteins and proteoforms in a small sample volume. Nevertheless, this method requires specialized equipment, extensive sample preparation, and highly trained technicians [3–5]. Due to simplicity of operation, rapidity, and cost-effectiveness, optical sensor arrays have emerged as promising alternatives for discrimination of chemically or structurally similar proteins, quantification of their levels, and identification of complex mixtures [6,7]. These sensing platforms usually consist of a set of chemical sensors that interact differently with protein analytes, generating unique response patterns for each. Chemometric tools such as principal component analysis (PCA), partial least squares discriminant

* Corresponding author.
** Corresponding author.
E-mail addresses: cssousa@ucp.pt (C. Sousa), lsaraiva@ff.up.pt (M.L.M.F.S. Saraiva).

https://doi.org/10.1016/j.dyepig.2022.110635
Received 9 June 2022; Received in revised form 27 July 2022; Accepted 1 August 2022
Available online 8 August 2022

Abbreviations

Alb	Albumin
Cat	Catalase
CD	Cyclodextrin
α-CD	Alpha-cyclodextrin
2-HP-β-CD	2-Hydroxypropyl-beta-cyclodextrin
γ-CD	Gamma-cyclodextrin
Cyt *c*	Cytochrome *c*
DLS	Dynamic light scattering
DMSO	Dimethylsulfoxide
EB	Erythrosin B
GUMBOS	Group of uniform materials based on organic salts
Hb	Hemoglobin
LV	Latent variable
Lyz	Lysozyme
PALS	Phase analysis light scattering
PCA	Principal component analysis
PDI	Polydispersity index
PLS	Partial least squares
PLSDA	Partial least squares discriminant analysis
P_{4444}	Tetrabutylphosphonium
RER	Range error ratio
RMSEC	Root mean square error of calibration
RMSECV	Root mean square error of cross-validation
RMSEP	Root mean square error of prediction
R^2C	Coefficient of determination of calibration
R^2CV	Coefficient of determination of cross-validation
R^2P	Coefficient of determination of prediction
SD	Standard deviation
SNV	Standard normal variate
TEM	Transmission electron microscopy
Try	Trypsin
UV–Vis	Ultraviolet–visible
ZP	Zeta potential

analysis (PLSDA), and partial least squares (PLS), may then be applied to extract relevant information from datasets [8,9]. However, widespread use of sensor arrays has been limited by the need for a large number of recognition elements as compared to proteins, which leads to high sample consumption as well as long acquisition and processing times [7,10]. There is a growing demand for simple sensor arrays composed of only a few sensing elements and/or single sensor systems, such as those that use multiple wavelengths to provide cross-reactive responses to proteins [11,12].

Various sensing scaffolds have been employed for protein analyses, including fluorescent dyes, conjugated polymers, and functionalized porphyrins [13–15]. More recently, nanoparticles have attracted considerable attention due to their unique optical properties, improved photochemical stability, and possibility of surface modification [16,17]. Despite these advantages, conventional nanoparticles often involve complex synthetic procedures, time-consuming purification steps, as well as expensive and hazardous chemicals [18,19]. The simplicity of preparation and high tunability of nanoparticles derived from a group of uniform materials based on organic salts (nanoGUMBOS) make them suitable candidates for detection and discrimination of proteins. Modulation of nanoGUMBOS properties may be achieved by changing the cation, anion, and alkyl chain length, thus eliminating the need for selective ligands while minimizing toxicity [20,21]. Furthermore, particle size may be controlled by simply adjusting experimental parameters such as concentration of GUMBOS solution, sonication time, and presence of template [22,23]. This is particularly relevant since it is known that size can affect nanoparticle-protein interactions [24,25].

In the study reported here, a phosphonium-erythrosin B-based nanoGUMBOS (i.e., $[P_{4444}]_2$[EB]) was synthesized using a simple ultrasound-assisted reprecipitation method, and its potential to discriminate and quantify various protein analytes was examined. The impact of sonication time and template choice on nanoGUMBOS size and, consequently, on its discriminatory power was assessed by PLSDA. Under optimized synthesis conditions, the ability of $[P_{4444}]_2$[EB] nanoGUMBOS to discriminate individual proteins at different concentrations (20.0–0.5 μg mL^{-1}) and protein mixtures was also examined. Moreover, PLS models were developed for protein quantification.

2. Experimental

2.1. Reagents and solvents

Tetrabutylphosphonium bromide ($[P_{4444}][Br]$, 98%); 2′,4′,5′,7′-tetraiodofluorescein disodium salt ($[Na]_2$[EB], 90%); alpha (α), 2-hydroxypropyl-beta (2-HP-β), and gamma (γ) CDs (≥98%); albumin (Alb) from human serum; human hemoglobin (Hb); trypsin (Try) from porcine pancreas; catalase (Cat) from bovine liver; lysozyme (Lyz) from chicken egg white; cytochrome *c* (Cyt *c*) from bovine heart; sodium phosphate dibasic (Na_2HPO_4); and sodium phosphate monobasic (NaH_2PO_4) were all obtained from Sigma-Aldrich (St. Louis, MO) and used as supplied. Dimethylsulfoxide (DMSO) was purchased from Merck KGaA (Darmstadt, Germany).

Phosphate buffer (10 mmol L^{-1}, pH 7.4) was obtained by dissolving Na_2HPO_4 and NaH_2PO_4 in ultrapure water (Milli-Q, 18.2 MΩ cm), and used for preparation of protein stock solutions. These solutions (300 μg mL^{-1}) were further diluted in phosphate buffer to obtain concentrations ranging from 20.0 to 0.5 μg mL^{-1}. Details of the synthesis and characterization of EB-based GUMBOS can be found in our previous study [26].

2.2. Synthesis of nanoGUMBOS

$[P_{4444}]_2$[EB] nanoGUMBOS were synthesized using an ultrasonication-assisted reprecipitation method (Fig. S1) [27]. Briefly, 200 μL of an 8 mmol L^{-1} solution of GUMBOS in DMSO were added to 9800 μL of ultrapure water with and without CD (1:1 M ratio). The mixture was then sonicated using an amplitude of 20% for 30 s, 5 min, and 15 min using a Vibra-Cell VCX 130 (Sonics & Materials, Inc., Newtown, CT) with a 6 mm diameter tip. Vials were kept in an ice bath during the procedure to avoid overheating.

2.3. Characterization of the synthesized nanoGUMBOS

Optical properties of $[P_{4444}]_2$[EB] nanoGUMBOS were investigated using UV–Vis spectroscopy. Absorbance measurements (300–700 nm) were performed on a Jasco V-660 spectrophotometer using a 1 cm quartz cuvette.

The hydrodynamic diameter, polydispersity index (PDI), and zeta potential (ZP) of synthesized nanoGUMBOS were determined using dynamic and phase analysis light scattering (DLS and PALS, respectively) with a ZetaPALS analyzer (Brookhaven Instruments, Holtsville, NY). Particle size and ZP measurements were performed at 25 °C with a detection angle of 90° and 15°, respectively. The number of runs per measurement was set to six (each with a duration of 2 min and 10 cycles, respectively), and the count rate was kept in the range of 300–500 kcps. Results were expressed as the mean ± standard deviation (SD) of three batches of nanoGUMBOS.

Transmission electron microscopy (TEM) analysis was performed to further examine the size and shape of $[P_{4444}]_2$[EB] nanoGUMBOS.

Briefly, an aliquot of 10 μL of nanoGUMBOS dispersion was placed on a formvar/carbon film-coated mesh nickel grid (Electron Microscopy Sciences, Hatfield, PA) and left standing for 2 min, after which excess liquid was removed using filter paper. Images were recorded using a JEM-1400 microscope (JEOL Ltd., Tokyo, Japan) operated at 120 kV and equipped with a CCD camera Orious 1100 W. Subsequently, the diameters of 100 randomly selected nanoGUMBOS were measured using ImageJ 1.53e (National Institutes of Health, Bethesda, MD), and data were fitted to a Gaussian function for determination of average particle size.

2.4. Evaluation of storage stability

The stability of $[P_{4444}]_2$[EB] nanoGUMBOS was assessed by monitoring changes in hydrodynamic diameter and PDI over eight weeks. For this study, nanoGUMBOS were stored in the dark at room temperature and DLS measurements were performed as described above.

2.5. Discrimination and quantification of proteins using nanoGUMBOS

In order to obtain maximum discrimination among proteins, the effect of sonication time and CD template on the discrimination performance of $[P_{4444}]_2$[EB] nanoGUMBOS was evaluated. Briefly, 20 μL of each protein sample (e.g., Alb, Hb, Try, Cat, Lyz, and Cyt *c*) were added to a 96-well microplate containing 80 μL of nanoGUMBOS dispersion and 200 μL of phosphate buffer pH 7.4. After a 5 min reaction period, UV–Vis spectra (Fig. 1) were recorded from 300 to 700 nm using a Cytation 3 imaging reader (BioTek Instruments, Winooski, VT). Protein and nanoGUMBOS concentrations were fixed at 20 μg mL^{-1} and 4 μmol L^{-1}, respectively.

Additional studies were performed to investigate the discrimination power of synthesized nanoGUMBOS at lower protein concentrations (15.0–0.5 μg mL^{-1}) as well as binary and ternary mixtures of Lyz, Cyt *c*, and Hb (total protein concentration = 6 μg mL^{-1}). Only $[P_{4444}]_2$[EB] nanoGUMBOS formed upon 5 min of sonication and in the absence of CD was used since these conditions resulted in better discrimination. The experimental procedure used for protein quantification was similar to that described above. For each protein, seven replicates were obtained.

2.6. Data analysis

Before modeling, all spectra were preprocessed using standard normal variate (SNV) [28], and then mean-centered. PLSDA was used to discriminate proteins and their mixtures at different concentrations/ratios, while PLS was used for predicting protein concentrations. The entire spectral wavelength range (300–700 nm) was considered in the analysis.

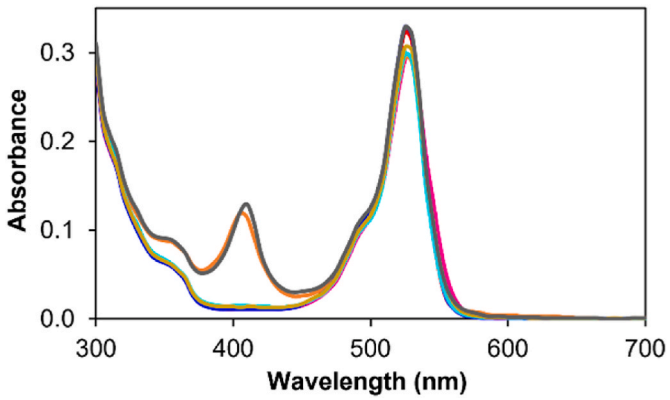

Fig. 1. Absorbance spectra of $[P_{4444}]_2$[EB] nanoGUMBOS (–) and $[P_{4444}]_2$[EB] nanoGUMBOS in the presence of Alb (–), Hb (–), Try (–), Cat (–), Lyz (–), and Cyt *c* (–). NanoGUMBOS were obtained after 5 min of sonication without CD.

PLSDA is a supervised classification method based on the PLS2 algorithm, which relies on prior knowledge of the data set [29,30]. In PLSDA, to each known sample (x_i, nanoGUMBOS spectra in the presence of a single protein) is assigned a vector of zeros with value one at the position corresponding to its class (y_i, in this study to each protein). The structure of the PLSDA model is described by Eqs. (1) and (2). Model loadings (P and Q) and corresponding scores (T and U) are obtained by sequentially extracting the components or latent variables (LVs) from matrices X (spectra) and Y (matrix codifying the proteins).

$$X = TP^t + E \quad (1)$$

$$Y = UQ^t + F \quad (2)$$

The algorithm correlates the scores of each block (T and U), yielding an internal regression matrix. This internal regression can be transformed on a regression matrix B. In this case, the regression matrix is composed of three vectors: one regression vector corresponding to each protein. E and F are the residual matrices and depend on the number of LVs selected. Predictions for new samples are obtained by multiplying a new spectrum (x_{new}) by the regression matrix B:

$$y_{new} = x_{new}\, B \quad (3)$$

The prediction ($y_{new} = [y_{new,1}, y_{new,2}, \ldots, y_{new,n}]$) is then converted into a class assignment (protein) from which confusion matrices are obtained. Before applying PLSDA, 70% of the samples are randomly selected to obtain the regression matrix B and 30% are used as new samples for prediction. This procedure is repeated 100 times per PLSDA model and confusion matrices present the mean values of correct protein assignments for the prediction samples.

During development of PLS models, samples were randomly separated into two sets: one for calibration + cross-validation (70%) and another for prediction (30%). The first set was further divided into a 70:30 ratio as described for PLSDA models. It is noted that the prediction set was totally independent, and never included in the calibration step (neither for calibration nor for cross-validation). The accuracy of PLS models was evaluated by calculating the coefficient of determination of calibration, cross-validation, and prediction (R^2C, R^2CV, and R^2P); the root mean square error of calibration, cross-validation, and prediction (RMSEC, RMSECV, and RMSEP); and the range error ratio (RER).

Data preprocessing and modeling were performed in MATLAB R2018b (MathWorks, Natick, MA) and PLS Toolbox 8.7 (Eigenvector Research, Manson, WA).

3. Results and discussion

3.1. Characterization of the synthesized nanoGUMBOS

Following synthesis, nanoGUMBOS properties were studied using UV–Vis spectroscopy, DLS/PALS, and TEM. As shown in Fig. S2, the synthesized nanoGUMBOS displayed similar absorption spectra to that of $[Na]_2$[EB] (parent dye) with an intense band at 527 nm, a shoulder at approximately 487 nm, and a lower intensity band around 310 nm [31,32]. Increased absorbance and spectral broadening is attributed to dye aggregation within nanoGUMBOS [33,34].

The results of particle size and ZP measurements are presented in Tables S1 and S2. Hydrodynamic diameters varied from 133 to 238 nm depending on sonication time and template choice. For example, templating with 2-HP-β-CD led to a reduction in particle size from 159 to 139 nm. PDI values were found to be lower than 0.2 for all synthesized nanoGUMBOS, indicating that particles are moderately polydisperse [35]. Examination of ZP data confirmed formation of highly stable nanoparticle dispersions (ZP ≥ -30 mV) [35]. The negative charge can be ascribed to adsorption of EB anion on the surface of nanoGUMBOS [22,23]. It is also worth noting that changes in sonication time and CD template did not significantly affect ZP, contrary to what was observed

for particle size.

TEM analysis revealed formation of quasi-spherical nanoparticles with an average diameter of 119 nm (Fig. S3). As expected, this value is lower than that obtained by DLS since it represents the size of nanoparticles in dry form [35,36]. It was also found that $[P_{4444}]_2$[EB] nanoGUMBOS remain stable for at least three weeks when stored in the dark at room temperature (Fig. S4).

3.2. Experimental optimization

3.2.1. Sonication time

The impact of sonication time on the discriminatory power of $[P_{4444}]_2$[EB] nanoGUMBOS was evaluated using six proteins, e.g., Alb, Hb, Try, Cat, Lyz, and Cyt *c* at the concentration of 20.0 μg mL^{-1}. These proteins were chosen as target analytes because they differ in abundance, hydrophobicity, isoelectric point, and molecular weight (Table S3). For example, Alb is the most abundant serum protein (normal concentration range = 35–50 mg mL^{-1}), displays higher surface hydrophobicity than Lyz, and has a molecular weight four times smaller as compared to Cat [37,38]. However, within this set of proteins, several pairs possess similar isoelectric points and molecular weights, which constitutes an additional challenge for discrimination of proteins using synthesized nanoGUMBOS.

Three PLSDA models, each corresponding to a single sonication time (30 s, 5 min, and 15 min), were developed as previously described in section 2.6. All scores maps showed six clusters, each related to a single protein, with varying degrees of overlap (Fig. 2). The first three LVs of PLSDA models encompassed around 99% of spectral variability and LV1 (≈90%) seemed to be responsible for discrimination between Hb + Cyt *c* and the remaining proteins. Alb was discriminated from Try, Cat, and Lyz on the second LV (LV2: 6–8% of spectral variability), being the last three proteins discriminated in different degrees along LV2 and LV3. The total percentages of correct protein assignments obtained from confusion matrices were: 96.4%–30 s, 99.6%–5 min, and 95.5%–15 min (Table 1). Alb, Hb, and Cyt *c* were 100% correctly predicted for the three sonication times. Try, Cat, and Lyz were misidentified mostly among each other, with the worst results obtained for 15 min of sonication. These findings demonstrate the impact of sonication time on discrimination performance of synthesized nanoGUMBOS. Moreover, surface charge, hydrophobicity, and size seem to affect the extent of interaction between $[P_{4444}]_2$[EB] nanoGUMBOS and protein analytes. Other studies confirm the role that these physicochemical properties play in discrimination of proteins [39,40]. The higher affinity of synthesized nanoGUMBOS for positively charged proteins (e.g., Alb and Hb) can be explained by its negative surface charge. Although hydrophobic and van der Waals interactions may also be involved, electrostatic interactions are thought to be the primary parameter responsible for protein discrimination [41,42]. Try and Lyz misidentifications can be attributed to similarity of their isoelectric points (10.5 *versus* 11.4). Additionally, the large molecular weight of Cat (250.0 kDa) can explain its reduced binding efficiency as compared to other positively charged proteins (Alb and Hb), and consequently, the lower percentages of correct predictions that were obtained [43].

3.2.2. CD templating

After fixing sonication time at 5 min, the ability of $[P_{4444}]_2$[EB] nanoGUMBOS to discriminate among proteins was evaluated in the presence of three CDs (α, 2-HP-β, and γ). The developed PLSDA models (Fig. S5) were quite similar to those obtained during optimization of sonication time, with six moderately separated clusters being observed (around 99% of spectral variability captured on the first three LVs). The corresponding confusion matrices were generated (Table S4) and the total percentages of correct protein assignments were shown in Fig. 3. Despite the high percentages of correct predictions obtained for all CD-templated nanoGUMBOS, the best result was achieved in the absence of CDs. Thus, it was decided to proceed with this study using non-

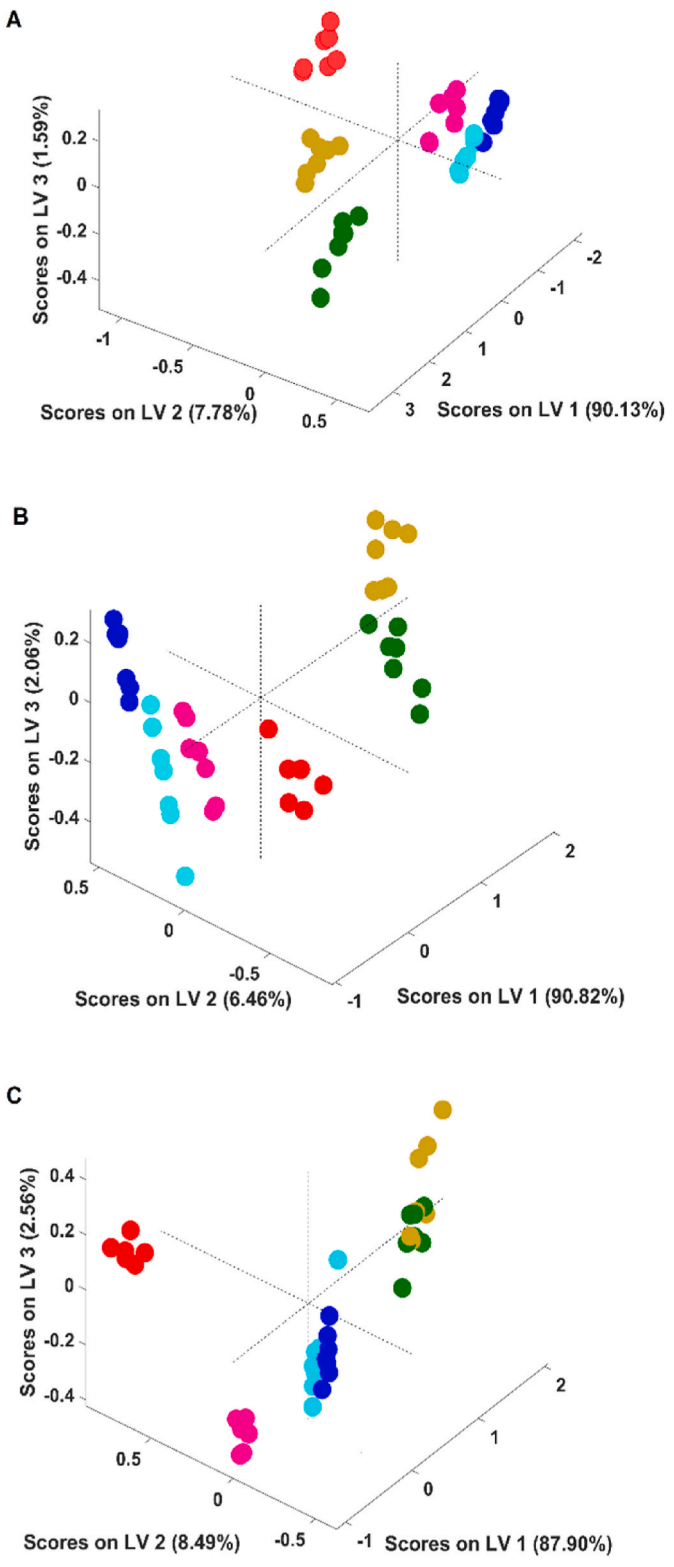

Fig. 2. Scores plots corresponding to the first three LVs of PLSDA regression models developed with UV–Vis spectra for protein discrimination: ● Alb, ● Hb, ● Try, ● Cat, ● Lyz, and ● Cyt *c*. $[P_{4444}]_2$[EB] nanoGUMBOS obtained after 30 s (A), 5 min (B), and 15 min (C) of sonication.

Table 1
Confusion matrices obtained from the PLSDA regression models developed for protein discrimination using the $[P_{4444}]_2[EB]$ nanoGUMBOS. Models A, B, and C correspond to 30 s, 5 min, and 15 min of sonication.

Model A	Alb	Hb	Try	Cat	Lyz	Cyt *c*	
Alb	16.67	0	0	0	0	0	–
Hb	0	16.67	0	0	0	0	–
Try	0	0	14.50	0.56	1.61	0	–
Cat	0	0	0.72	15.94	0	0	–
Lyz	0	0	0.11	0.56	16.00	0	–
Cyt *c*	0	0	0	0	0	16.67	–
Correct protein discrimination (%)							**96.4**
Model B	Alb	Hb	Try	Cat	Lyz	Cyt *c*	
Alb	16.67	0	0	0	0	0	–
Hb	0	16.67	0	0	0	0	–
Try	0	0	16.61	0.06	0	0	–
Cat	0.11	0	0.06	16.50	0	0	–
Lyz	0.11	0	0	0.06	16.50	0	–
Cyt *c*	0	0	0	0	0	16.67	–
Correct protein discrimination (%)							**99.6**
Model C	Alb	Hb	Try	Cat	Lyz	Cyt *c*	
Alb	16.67	0	0	0	0	0	–
Hb	0	16.67	0	0	0	0	–
Try	0	0	15.56	0.61	0.50	0	–
Cat	0	0	3.22	13.39	0.06	0	–
Lyz	0	0	0.06	0.06	16.56	0	–
Cyt *c*	0	0	0	0	0	16.67	–
Correct protein discrimination (%)							**95.5**

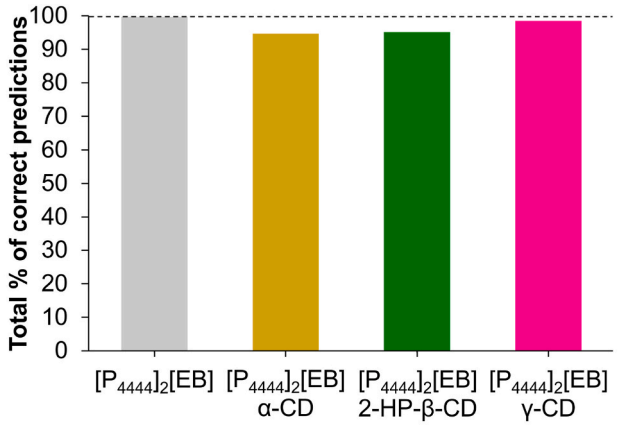

Fig. 3. Total percentages of correct protein discrimination obtained with the $[P_{4444}]_2[EB]$ nanoGUMBOS synthesized in the absence and presence of three CDs (α, 2-HP-β, and γ).

templated nanoGUMBOS.

3.3. Discrimination of proteins and their concentrations

Optimization of sonication time and assessment of impact of CDs on discrimination success was performed at a protein concentration of 20.0 μg mL^{-1}. Additional studies were performed to evaluate the ability of $[P_{4444}]_2[EB]$ nanoGUMBOS to distinguish lower concentrations of proteins (15.0–0.5 μg mL^{-1}). For each concentration, a PLSDA model was developed (data not shown) and a corresponding confusion matrix was obtained (more details in section 2.6). Despite encompassing high spectral variability in the first three LVs (≈96–99%), the degree of clusters overlapping increased for lower concentrations of proteins. This finding was consistent with smaller percentages of correct protein assignments obtained from confusion matrices (Fig. 4). $[P_{4444}]_2[EB]$ nanoGUMBOS was able to discriminate between 70 and 80% of the

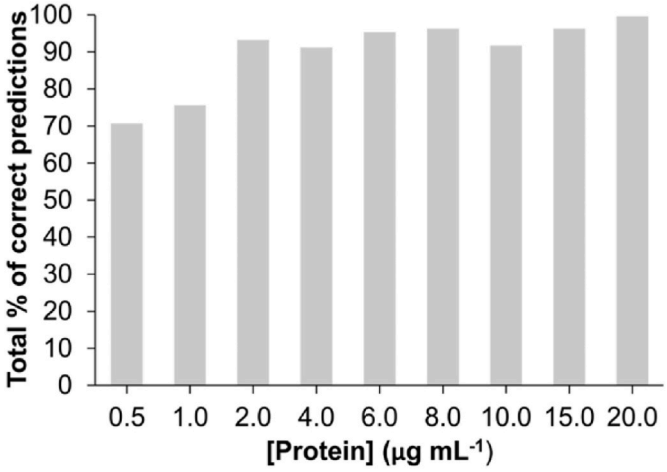

Fig. 4. Total percentages of correct protein assignments obtained with the $[P_{4444}]_2[EB]$ nanoGUMBOS at various protein concentrations.

protein samples with concentrations of 0.5 and 1.0 μg mL^{-1}. Additionally, there was an improvement in discrimination performance of nanoGUMBOS for concentrations higher than 1.0 μg mL^{-1} (percentage of correct discriminations >90%). Only small fluctuations occurred in total percentages of correct protein predictions from 2.0 to 20.0 μg mL^{-1}, with maximum (99.6%) being obtained for the highest concentration tested. In fact, this nanoGUMBOS approach produces a very satisfactory percentage of correct identifications for lower concentrations of proteins as compared to those reported for other sensing systems [44–47]. Moreover, it requires only 5 min of reaction time and one probe to discriminate among all protein samples.

Regarding each protein individually (Table 2), Hb and Cyt *c* seemed to be the best predicted in the whole concentration range (percentage of correct predictions ≥99% for [Protein] ≥ 2.0 μg mL^{-1}). Cat was the worst predicted (75.3–91.7%), reaching 99.0% of correct prediction only for [Protein] = 20.0 μg mL^{-1}. Alb, Try, and Lyz presented random fluctuations in the percentages of correct discriminations across the concentration range, being the worst result obtained for Lyz at 1.0 μg mL^{-1} (52.0%) and the best result found for Alb at the concentration of 20.0 μg mL^{-1} (100% of correct predictions).

3.4. Discrimination of binary and ternary mixtures of Lyz, Cyt c, and Hb

The ability of $[P_{4444}]_2[EB]$ nanoGUMBOS to discriminate between mixtures of Lyz + Cyt *c*, Lyz + Hb, Cyt *c* + Hb, and Lyz + Cyt *c* + Hb was also evaluated. For each protein mixture, a PLSDA model was developed and scores maps were obtained (Fig. 5). Regarding Lyz + Cyt *c*, the first two LVs of the PLSDA model (Fig. 5A) encompassed 99% of spectral variability, being the samples discriminated across LV1. Pure Lyz and Cyt *c* samples were located on opposite sides of the scores map (positive

Table 2
Percentages of correct predictions (%) for different concentrations of proteins obtained from the confusion matrices of PLSDA regression models.

[Protein] (μg mL^{-1})	Correct protein predictions (%)					
	Alb	Hb	Try	Cat	Lyz	Cyt *c*
0.5	62.0	70.0	76.3	76.7	65.3	74.0
1.0	70.7	83.0	99.0	75.3	52.0	73.7
2.0	91.3	98.7	99.0	80.7	89.7	100.0
4.0	97.0	100.0	74.3	79.3	96.7	100.0
6.0	99.0	100.0	93.7	79.0	100.0	100.0
8.0	100.0	100.0	90.3	88.0	99.3	100.0
10.0	66.7	100.0	79.3	87.0	86.3	100.0
15.0	100.0	100.0	93.0	91.7	93.3	100.0
20.0	100.0	100.0	99.7	99.0	99.0	100.0

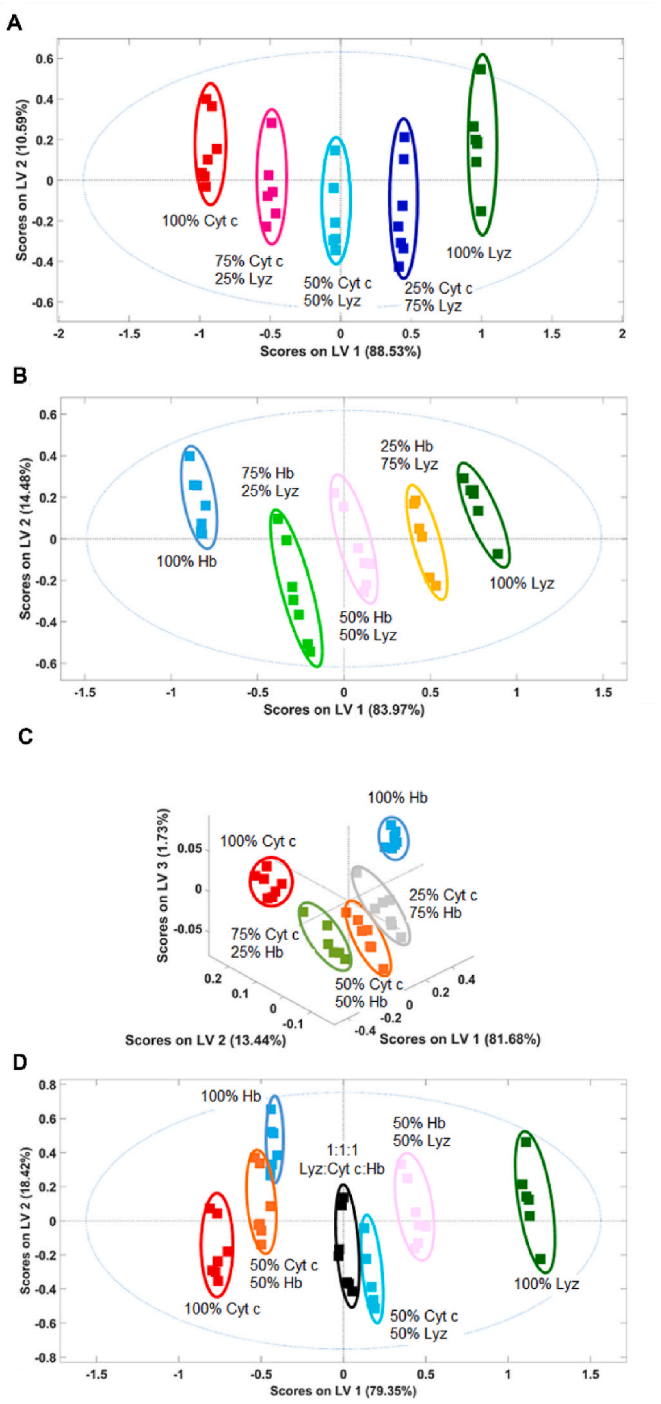

Fig. 5. Scores plots of PLSDA regression models developed with UV–Vis spectra of $[P_{4444}]_2$[EB] nanoGUMBOS incubated with mixtures of (A) Lyz and Cyt *c*; (B) Lyz and Hb; (C) Cyt *c* and Hb; and (D) Lyz, Cyt *c*, and Hb. Legend: ■ 100% Lyz; ■ 100% Cyt *c*; ■ 100% Hb; ■ 75% Lyz +25% Cyt *c*; ■ 50% Lyz +50% Cyt *c*; ■ 25% Lyz +75% Cyt *c*; ■ 25% Lyz +75% Hb; ■ 50% Lyz +50% Hb; ■ 75% Lyz +25% Hb; ■ 50% Cyt *c* + 50% Hb; ■ 75% Cyt *c* + 25% Hb; ■ 75% Cyt *c* + 25% Hb; ■ 1:1:1, Lyz:Cyt *c*:Hb.

and negative, respectively), while mixed samples appeared between them. It is noted that samples possessing 50% of each protein were precisely located in the middle of the scores map (0 of the LV1 axis) and that those containing 75% + 25% were closer to the corresponding pure protein. This clear separation of samples corroborates previous results concerning discrimination of single proteins. Lyz and Cyt *c* were also easily discriminated between each other, appearing on opposite sides of the first LV of scores map. Regarding the mixture of Lyz and Hb (Fig. 5B), a quite similar result was obtained. Pure samples of Lyz and Hb appeared on opposite sides of LV1, with mixed samples located between them according to protein ratio. Hb was located near Cyt *c* in the scores map when the six proteins were discriminated simultaneously (Fig. 1B), which somehow justifies the similar results of Lyz + Cyt *c* and Lyz + Hb mixtures. In this context, it was decided to evaluate the ability of $[P_{4444}]_2$[EB] nanoGUMBOS to discriminate between protein mixtures of Hb and Cyt *c*. The scores plot obtained from the corresponding PLSDA model (Fig. 5C) showed considerably overlapped clusters when only the first two LVs were used (data not shown). In contrast to previously studied mixtures, use of the third LV was mandatory for clusters separation. Considering the three LVs, it was possible to observe five individualized clusters, which were located in the scores map according to the ratio of proteins in the mixture. Results obtained for this mixture were in good agreement with the already mentioned closeness of Hb and Cyt *c* when the six proteins were discriminated simultaneously. An additional study was performed to evaluate the behavior of $[P_{4444}]_2$[EB] nanoGUMBOS towards a ternary mixture of Lyz, Cyt *c*, and Hb (1:1:1, Fig. 5D). The scores map of the PLSDA model confirmed conclusions noted above. Separation of pure samples of Lyz, Cyt *c*, and Hb was observed in the first LV, confirming the high structural similarity between Cyt *c* and Hb previously reported in the literature [48]. Moreover, 50:50 mixtures of these proteins were located in the scores map near the middle of pure samples. Regarding the ternary mixture (Lyz:Cyt *c*:Hb), samples were not in a central position between pure proteins (Fig. 5D). They seemed to be quite closer to pure Hb and Cyt *c* samples, and more separate from Lyz. However, this location in the scores map was expected since two pure samples (Hb and Cyt *c*) appeared on the negative side of LV1, while only one (Lyz) was located on the positive side.

3.5. Protein quantitative analysis

Regarding protein discrimination using $[P_{4444}]_2$[EB] nanoGUMBOS, a very satisfactory percentage of correct assignments (>90%) was achieved for concentrations ranging from 2.0 to 20.0 μg mL^{-1}. Therefore, it was decided to evaluate the ability of this nanoGUMBOS to quantify each protein separately in the mentioned concentration range. Six PLS models (one for each protein) were developed, being the number of LVs selected from the RMSECV plots (Fig. S6, A–F). The figures of merit obtained are presented in Table 3. Overall, the PLS model developed for Alb quantification provided the best performance. Despite having a slightly higher RMSEC than Try (6.5 *versus* 4.5%), the corresponding RMSECV was the lowest in this study (7.8%). The R^2C and R^2CV obtained for Alb were also the highest ones (0.99 for both). In contrast, the PLS model developed for Cat quantification showed the worst performance with a RMSEC of 10.4% (R^2C = 0.97) and a RMSECV of 26.8% (R^2CV = 0.83). The remaining four proteins presented intermediate RMSEC values (Hb = 9.8%, Try = 4.5%, Lyz = 7.3%, and Cyt *c* = 8.2%) and very good calibration coefficients of determination (0.98–0.99). Additionally, the errors of cross-validation set (RMSECV) were lower than those obtained for calibration (Hb = 18.5%, Try = 16.0%, Lyz = 14.3%, and Cyt *c* = 19.3%), with R^2CV ranging from 0.91 to 0.94. All PLS models developed were validated using an independent set of samples (the prediction set P), which was randomly selected from initial data and never used in the calibration or cross-validation steps. This set of samples further allowed testing of the robustness of the PLS models. Although coefficients of determination obtained for the prediction set were quite good (0.88–0.97); for Cat, the value was only 0.78. Root mean square errors were quite variable and followed a similar trend to that observed for the cross-validation set (8.9–28.1%), being the best performance achieved for quantification of Alb. Regarding RER, the worst results were obtained for Hb and Cat (below 10). For Try, Lyz, and Cyt *c*, 15 > RER ≥10, suggesting that the developed models are suitable for calibration and quality control. The RER value obtained for Alb was 21.6, indicating that the model is appropriate for quantification (RER

Table 3
Figures of merit obtained from the PLS models developed to predict protein concentration (20.0 ≥ [Protein] ≥ 2.0 μg mL^{-1}) using the $[P_{4444}]_2$[EB] nanoGUMBOS.

Protein	LVs	RMSEC	R^2C	RMSECV	R^2CV	RMSEP	R^2P	RER
Alb	4	0.60	0.99	0.72	0.99	0.83	0.97	21.6
Hb	6	0.91	0.98	1.72	0.93	1.92	0.88	9.4
Try	6	0.42	0.99	1.49	0.94	1.46	0.95	12.3
Cat	6	0.97	0.97	2.49	0.83	2.61	0.78	6.9
Lyz	5	0.68	0.99	1.33	0.94	1.15	0.97	15.7
Cyt *c*	6	0.76	0.98	1.79	0.91	1.37	0.95	13.1

Latent variable (LV); Root mean square error of calibration (RMSEC), cross-validation (RMSECV), and prediction (RMSEP); Coefficient of determination of calibration (R^2C), cross-validation (R^2CV), and prediction (R^2P); RER = Δy/RMSEP.

≥15) [49].

4. Conclusions

This study focused on development of an alternative strategy to discriminate and quantify proteins. A phosphonium-erythrosin B-based nanoGUMBOS was synthesized using a simple reprecipitation method and its discrimination performance was optimized by varying sonication time (30 s–15 min) and CD template (α, 2-HP-β, or γ). The percentages of correct protein assignments varied from 94.6 to 99.6%, with best results obtained when sonication time was set to 5 min and using no template. Under these conditions, it was possible to discriminate proteins at various concentrations (from 20.0 to 2.0 μg mL^{-1}) and distinguish between mixtures of Lyz, Cyt *c*, and Hb at different proportions (25% + 50%, 50% + 50%, 75% + 25%, and 1:1:1). Regarding protein quantification, the models developed for Alb and Cat showed the best and worst performance, respectively. The PLS model obtained for Alb (RER = 21.6) proved also to be suitable for quantification purposes, while those developed for Try, Lyz, and Cyt *c* seemed to be appropriate for calibration and quality control (15 > RER ≥10). Overall, the obtained results demonstrated that the proposed strategy holds great promise for rapid discrimination of single proteins and their mixtures at different concentrations/ratios as well as quantification of Alb. Moreover, this approach is label-free, requires only one probe to discriminate all protein samples, and involves use of small volumes of reagents, which make this strategy attractive for high-throughput applications. Future studies include analysis of other proteins of interest and biofluids such as blood and urine.

CRediT authorship contribution statement

Ana M.O. Azevedo: Conceptualization, Methodology, Investigation, Writing – original draft. **Clara Sousa:** Formal analysis, Writing – original draft, Writing – review & editing. **S. Sofia M. Rodrigues:** Investigation. **Mi Chen:** Methodology. **Caitlan E. Ayala:** Writing – review & editing. **Rocío L. Pérez:** Writing – review & editing. **João L.M. Santos:** Conceptualization, Supervision. **Isiah M. Warner:** Conceptualization, Writing - review & editing, Supervision. **M. Lúcia M.F.S. Saraiva:** Conceptualization, Writing – review & editing, Supervision.

Declaration of competing interest

The authors declare that they have no known competing financial interests or personal relationships that could have appeared to influence the work reported in this paper.

Data availability

Data will be made available on request.

Acknowledgments

This work received financial support from PT national funds (FCT/MCTES, Fundação para a Ciência e Tecnologia and Ministério da Ciência, Tecnologia e Ensino Superior) through the projects UIDB/50006/2020, UIDB/50016/2020, and UIDP/50006/2020. It was also supported by the European Union (FEDER funds through the Operational Competitiveness Program (COMPETE) POCI-01-0145-FEDER-030163 – Project Tailored NanoGUMBOS: The green key to wound infections chemsensing).

Ana M.O. Azevedo thanks FCT and FSE (Fundo Social Europeu) through Programa Operacional Regional do Norte for her PhD grant with reference number SFRH/BD/118566/2016. Isiah M. Warner acknowledges support from the National Science Foundation (NSF) under grant # CHE-1905105. The opinions, findings, and conclusions or recommendations expressed are those of the authors and do not necessarily reflect the views of NSF.

TEM was performed at the HEMS core facility at i3S, Universidade do Porto, Portugal, with the assistance of Ana Rita Malheiro and Rui Fernandes.

Appendix A. Supplementary data

Supplementary data to this article can be found online at https://doi.org/10.1016/j.dyepig.2022.110635.

References

[1] Motiei L, Pode Z, Koganitsky A, Margulies D. Targeted protein surface sensors as a tool for analyzing small populations of proteins in biological mixtures. Angew. Chem.-Int. Edit. 2014;53:9289–93. https://doi.org/10.1002/anie.201402501.
[2] Fang Z, Liu LP, Wang Y, Xi DM, Zhang SS. Unambiguous discrimination of multiple protein biomarkers by nanopore sensing with double-stranded DNA-based probes. Anal Chem 2020;92:1730–7. https://doi.org/10.1021/acs.analchem.9b02965.
[3] Kingsmore SF. Multiplexed protein measurement: technologies and applications of protein and antibody arrays. Nat Rev Drug Discov 2006;5:310–20. https://doi.org/10.1038/nrd2006.
[4] Donnelly DP, Rawlins CM, DeHart CJ, Fornelli L, Schachner LF, Lin ZQ, Lippens JL, Aluri KC, Sarin R, Chen BF, Lantz C, Jung W, Johnson KR, Koller A, Wolff JJ, Campuzano IDG, Auclair JR, Ivanov AR, Whitelegge JP, Pasa-Tolic L, Chamot-Rooke J, Danis PO, Smith LM, Tsybin YO, Loo JA, Ge Y, Kelleher NL, Agar JN. Best practices and benchmarks for intact protein analysis for top-down mass spectrometry. Nat Methods 2019;16:587–94. https://doi.org/10.1038/s41592-019-0457-0.
[5] Smit NPM, Ruhaak LR, Romijn FPHTM, Pieterse MM, van der Burgt YEM, Cobbaert CM. The time has come for quantitative protein mass spectrometry tests that target unmet clinical needs. J Am Soc Mass Spectrom 2021;32:636–47. https://doi.org/10.1021/jasms.0c00379.
[6] Hou CJ, Dong JL, Zhang GP, Lei Y, Yang M, Zhang YC, Liu Z, Zhang SY, Huo DQ. Colorimetric artificial tongue for protein identification. Biosens Bioelectron 2011;26:3981–6. https://doi.org/10.1016/j.bios.2010.11.025.
[7] Fan JM, Qi L, Han HF, Ding LP. Array-based discriminative optical biosensors for identifying multiple proteins in aqueous solution and biofluids. Front Chem 2020;8:18. https://doi.org/10.3389/fchem.2020.572234.
[8] Umali AP, Anslyn EV. A general approach to differential sensing using synthetic molecular receptors. Curr Opin Chem Biol 2010;14:685–92. https://doi.org/10.1016/j.cbpa.2010.07.022.
[9] Martynko E, Kirsanov D. Application of chemometrics in biosensing: a brief review. Biosens Bioelectron 2020;10:20. https://doi.org/10.3390/bios10080100.
[10] Fan JM, Ding LP. Single-system based discriminative optical sensors: different strategies and versatile applications. Analyst 2018;143:3775–88. https://doi.org/10.1039/c8an00235e.
[11] Zheng DM, Fan JM, Huang XY, Ding LP, Xin YH. Fluorescent binary ensemble with pattern recognition ability for identifying multiple metalloproteins with applications in serum and urine. RSC Adv 2017;7:50097–105. https://doi.org/10.1039/c7ra09741g.

[12] Fan JM, Zheng DM, Huang XY, Ding LP, Xin YH, Fang Y. A single discriminative sensor based on supramolecular self-assemblies of an amphiphilic cholic acid-modified fluorophore for identifying multiple proteins. Sens. Actuator B-Chem. 2018;263:336–46. https://doi.org/10.1016/j.snb.2018.02.132.
[13] Perez RL, Cong MY, Vaughan SR, Ayala CE, Galpothdeniya WIS, Mathaga JK, Warner IM. Protein discrimination using a fluorescence-based sensor array of thiacarbocyanine-GUMBOS. ACS Sens 2020;5:2422–9. https://doi.org/10.1021/acssensors.0c00484.
[14] Miranda OR, You CC, Phillips R, Kim IB, Ghosh PS, Bunz UHF, Rotello VM. Array-based sensing of proteins using conjugated polymers. J Am Chem Soc 2007;129:9856–7. https://doi.org/10.1021/ja0737927.
[15] Zhou HC, Baldini L, Hong J, Wilson AJ, Hamilton AD. Pattern recognition of proteins based on an array of functionalized porphyrins. J Am Chem Soc 2006;128:2421–5. https://doi.org/10.1021/ja056833c.
[16] Miranda OR, Creran B, Rotello VM. Array-based sensing with nanoparticles: 'Chemical noses' for sensing biomolecules and cell surfaces. Curr Opin Chem Biol 2010;14:728–36. https://doi.org/10.1016/j.cbpa.2010.07.021.
[17] Bigdeli A, Ghasemi F, Golmohammadi H, Abbasi-Moayed S, Nejad MAF, Fahimi-Kashani N, Jafarinejad S, Shahrajabian M, Hormozi-Nezhad MR. Nanoparticle-based optical sensor arrays. Nanoscale 2017;9:16546–63. https://doi.org/10.1039/c7nr03311g.
[18] Ravichandran V, Vasanthi S, Shalini S, Shah SAA, Tripathy M, Paliwal N. Green synthesis, characterization, antibacterial, antioxidant and photocatalytic activity of Parkia speciosa leaves extract mediated silver nanoparticles. Results Phys 2019;15:8. https://doi.org/10.1016/j.rinp.2019.102565.
[19] Cao Y, Dhahad HA, El-Shorbagy MA, Alijani HQ, Zakeri M, Heydari A, Bahonar E, Slouf M, Khatami M, Naderifar M, Iravani S, Khatami S, Dehkordi FF. Green synthesis of bimetallic ZnO-CuO nanoparticles and their cytotoxicity properties. Sci Rep 2021;11:8. https://doi.org/10.1038/s41598-021-02937-1.
[20] Bhattarai N, Chen M, Perez RL, Ravula S, Strongin RM, McDonough K, Warner IM. Comparison of chemotherapeutic activities of rhodamine-based GUMBOS and NanoGUMBOS. Molecules 2020;25:13. https://doi.org/10.3390/molecules25143272.
[21] Azevedo AMO, Santos JLM, Warner IM, Saraiva MLMFS. GUMBOS and nanoGUMBOS in chemical and biological analysis: a review. Anal Chim Acta 2020;1133:180–98. https://doi.org/10.1016/j.aca.2020.06.028.
[22] Hamdan S, Dumke JC, El-Zahab B, Das S, Boldor D, Baker GA, Warner IM. Strategies for controlled synthesis of nanoparticles derived from a group of uniform materials based on organic salts. J Colloid Interface Sci 2015;446:163–9. https://doi.org/10.1016/j.jcis.2015.01.023.
[23] Chen M, Bhattarai N, Cong MY, Perez RL, McDonough KC, Warner IM. Mitochondria targeting IR780-based nanoGUMBOS for enhanced selective toxicity towards cancer cells. RSC Adv 2018;8:31700–9. https://doi.org/10.1039/c8ra05484c.
[24] Deng ZJ, Liang MT, Toth I, Monteiro MJ, Minchin RF. Molecular interaction of poly (acrylic acid) gold nanoparticles with human fibrinogen. ACS Nano 2012;6:8962–9. https://doi.org/10.1021/nn3029953.
[25] Saptarshi SR, Duschl A, Lopata AL. Interaction of nanoparticles with proteins: relation to bio-reactivity of the nanoparticle. J Nanobiotechnol 2013;11:12. https://doi.org/10.1186/1477-3155-11-26.
[26] Azevedo AMO, Sousa C, Chen M, Ayala CE, Perez RL, Santos JLM, Warner IM, Saraiva MLMFS. Protein discrimination using erythrosin B-based GUMBOS in combination with UV–Vis spectroscopy and chemometrics. Talanta 2022;240:123164. https://doi.org/10.1016/j.talanta.2021.123164.
[27] Cong MY, Perez RL, Chen M, Chapai R, Jin RY, Vidanapathirana P, Warner IM. Imidazolium-dysprosium-based magnetic NanoGUMBOS for isolation of hemoglobin. Talanta 2019;205:120078. https://doi.org/10.1016/j.talanta.2019.06.078.
[28] Naes T, Isaksson T, Fearn T, Davies T. A user-friendly guide to multivariate calibration and classification. Chichester, UK: NIR Publications; 2002.
[29] Geladi P, Kowalski BR. Partial least-squares regression: a tutorial. Anal Chim Acta 1986;185:1–17. https://doi.org/10.1016/0003-2670(86)80028-9.
[30] Alsberg BK, Kell DB, Goodacre R. Variable selection in discriminant partial least-squares analysis. Anal Chem 1998;70:4126–33. https://doi.org/10.1021/ac980506o.
[31] Fleming GR, Knight AWE, Morris JM, Morrison RJS, Robinson GW. Picosecond fluorescence studies of xanthene dyes. J Am Chem Soc 1977;99:4306–11. https://doi.org/10.1021/ja00455a017.
[32] Montero E, Garcia MA, Villegas MA, Llopis J. Spectral pH dependence of erythrosin B in sol-gel silica coatings and buffered solutions. Bol. Soc. Esp. Ceram. Vidr. 2008;47:1–6. https://doi.org/10.3989/cyv.2008.v47.i1.205.
[33] Dahne L. Self-organization of polymethine dyes in thin solid layers. J Am Chem Soc 1995;117:12855–60. https://doi.org/10.1021/ja00156a024.
[34] Das S, Bwambok D, El-Zahab B, Monk J, de Rooy SL, Challa S, Li M, Hung FR, Baker GA, Warner IM. Nontemplated approach to tuning the spectral properties of cyanine-based fluorescent NanoGUMBOS. Langmuir 2010;26:12867–76. https://doi.org/10.1021/la101463r.
[35] Bhattacharjee S. DLS and zeta potential - what they are and what they are not? J Contr Release 2016;235:337–51. https://doi.org/10.1016/j.jconrel.2016.06.017.
[36] Mourdikoudis S, Pallares RM, Thanh NTK. Characterization techniques for nanoparticles: comparison and complementarity upon studying nanoparticle properties. Nanoscale 2018;10:12871–934. https://doi.org/10.1039/c8nr02278j.
[37] Anderson NL, Anderson NG. The human plasma proteome - history, character, and diagnostic prospects. Mol Cell Proteomics 2002;1:845–67. https://doi.org/10.1074/mcp.R200007-MCP200.
[38] Nicolau DV, Paszek E, Fulga F, Nicolau DV. Mapping hydrophobicity on the protein molecular surface at atom-level resolution. PLoS One 2014;9:28. https://doi.org/10.1371/journal.pone.0114042.
[39] You CC, Miranda OR, Gider B, Ghosh PS, Kim IB, Erdogan B, Krovi SA, Bunz UHF, Rotello VM. Detection and identification of proteins using nanoparticle-fluorescent polymer 'chemical nose' sensors. Nat Nanotechnol 2007;2:318–23. https://doi.org/10.1038/nnano.2007.99.
[40] Li XN, Wen F, Creran B, Jeong YD, Zhang XR, Rotello VM. Colorimetric protein sensing using catalytically amplified sensor arrays. Small 2012;8:3589–92. https://doi.org/10.1002/smll.201201549.
[41] Ganesan L, Margolles-Clark E, Song Y, Buchwald P. The food colorant erythrosine is a promiscuous protein-protein interaction inhibitor. Biochem Pharmacol 2011;81:810–8. https://doi.org/10.1016/j.bcp.2010.12.020.
[42] Wang FY, Lu YX, Yang JC, Chen Y, Jing WJ, He LY, Liu YY. A smartphone readable colorimetric sensing platform for rapid multiple protein detection. Analyst 2017;142:3177–82. https://doi.org/10.1039/c7an00990a.
[43] Joseph A, Nyambura CW, Bondurant D, Corry K, Beebout D, Wood TR, Pfaendtner J, Nance E. Formulation and efficacy of catalase-loaded nanoparticles for the treatment of neonatal hypoxic-ischemic encephalopathy. Pharmaceutics 2021;13:17. https://doi.org/10.3390/pharmaceutics13081131.
[44] Kong H, Liu D, Zhang SC, Zhang XR. Protein sensing and cell discrimination using a sensor array based on nanomaterial-assisted chemiluminescence. Anal Chem 2011;83:1867–70. https://doi.org/10.1021/ac200076c.
[45] Xu SH, Lu X, Yao CX, Huang F, Jiang H, Hua WH, Na N, Liu HY, Ouyang J. A visual sensor array for pattern recognition analysis of proteins using novel blue-emitting fluorescent gold nanoclusters. Anal Chem 2014;86:11634–9. https://doi.org/10.1021/ac502643s.
[46] Xu SH, Wu YF, Sun XM, Wang ZQ, Luo XL. A multicoloured Au NCs based cross-reactive sensor array for discrimination of multiple proteins. J Math Chem B 2017;5:4207–13. https://doi.org/10.1039/c7tb00367f.
[47] Shen YS, Huang YF, Zhang PMM, Guo BC, Jiang HT, Tan CY, Jiang YY. Fluorescence sensor array for discrimination of urine proteins and differentiation diagnosis of urinary system diseases. ACS Appl Bio Mater 2020;3:5639–43. https://doi.org/10.1021/acsabm.0c00845.
[48] Chertkova RV, Brazhe NA, Bryantseva TV, Nekrasov AN, Dolgikh DA, Yusipovich AI, Sosnovtseva O, Maksimov GV, Rubin AB, Kirpichnikov MP. New insight into the mechanism of mitochondrial cytochrome c function. PLoS One 2017;12:20. https://doi.org/10.1371/journal.pone.0178280.
[49] AACC. Near-infrared methods – guidelines for model development and maintenance. St. Paul, MN: AACC Press; 1999.